9
Localized surface plasmons

Figures

9.1 Nanoparticles

9.1.1 Introduction

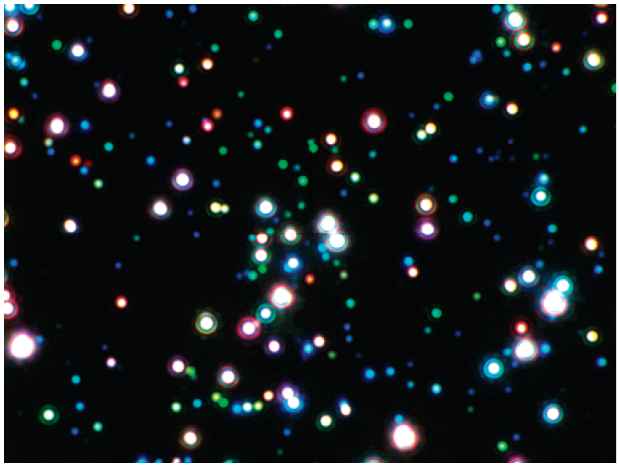

Fig. 9.1. Dark field image (130×170 μm) of light scattered from silver particles with an average diameter of 35 nm. Reprinted with permission from reference [1], © 2003 American Chemical Society.

9.1.2 Mie theory examples

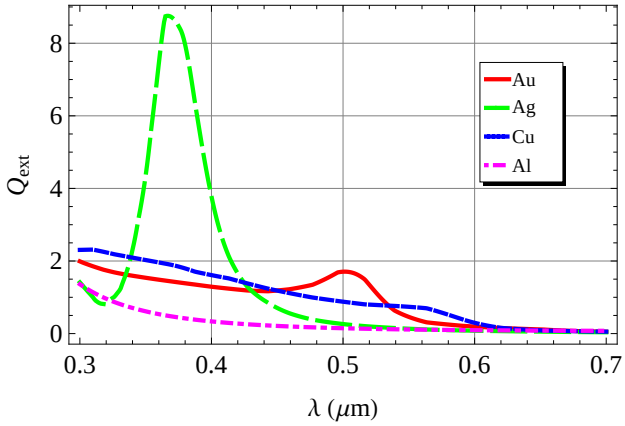

Fig. 9.2. Extinction coefficient as a function of wavelength, λ, for a 60 nm sphere made of gold (solid line), silver (long dashes), copper (short dashes) or aluminum (dot dashes) in air. The extinction is dominated by the dipole resonance. (Mathematica simulation)

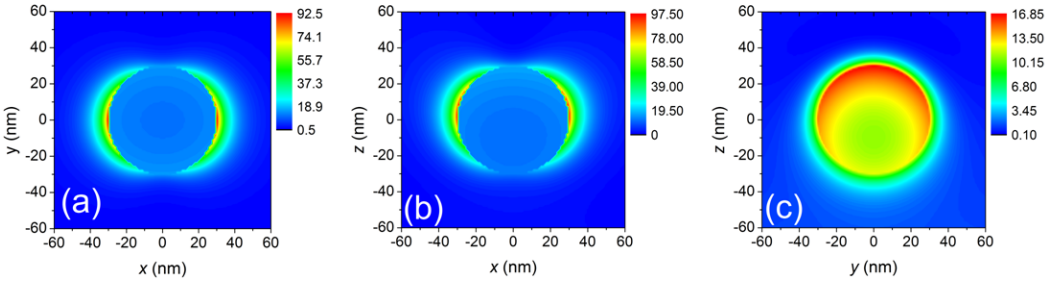

Fig. 9.3. The field intensity, $|E|^2$, in the vicinity of a 60 nm silver sphere in air at the resonance wavelength of 367 nm when excited by a plane wave of unit amplitude traveling in the -*z*-direction and polarized along the *x*-direction. The refractive index for silver in this Mie calculation is 0.189 + 1.622*i*.

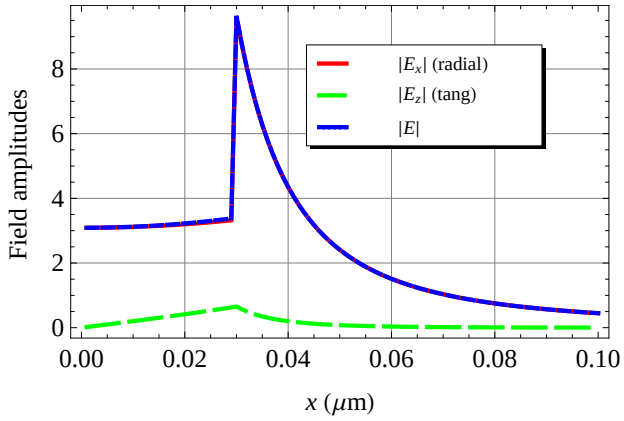

Fig. 9.4. Electric field components along the *x*-axis in Fig. 9.3(b). $|E|$ (dotted) and $|E_x|$ (solid line) nearly overlap, while $|E_z|$ (dashed) is much smaller. (*Mathematica* simulation)

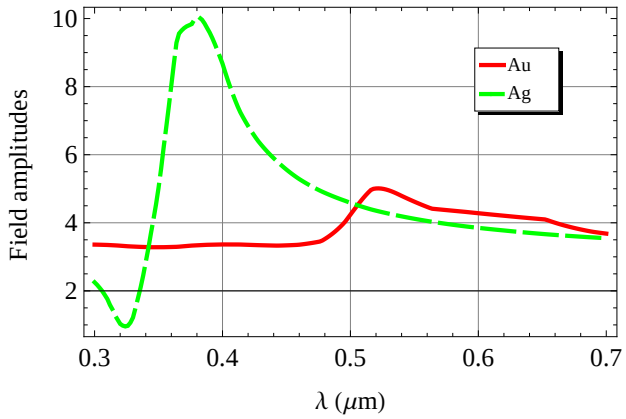

Fig. 9.5. Field amplitude on the surface of a nanosphere centered on the origin where the surface intersects the *x*-axis for a 60-nm diameter gold (solid line) and silver (dashed) sphere in air as a function of wavelength, λ. The incident beam is travelling in the *z*-direction and is polarized in the *x*-direction. (*Mathematica* simulation)

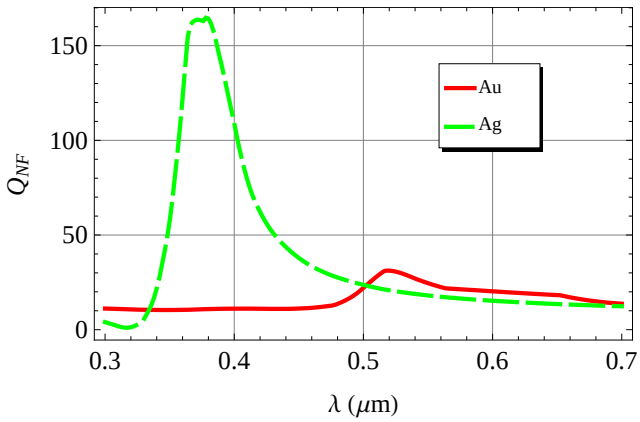

Fig. 9.6. Near field coefficient for a 60-nm diameter gold (solid line) and silver (dashed) sphere in air as a function of wavelength, λ. (*Mathematica* simulation)

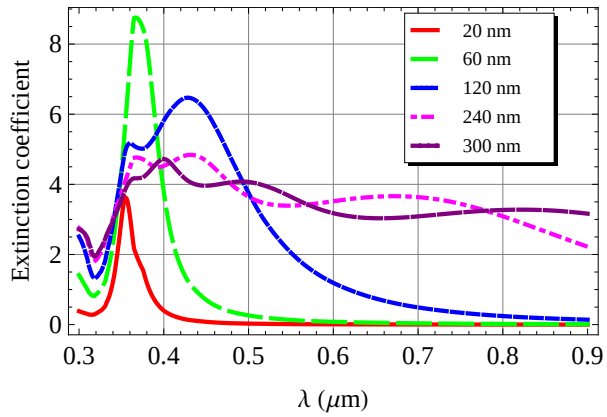

Fig. 9.7. Extinction coefficient as a function of wavelength, λ, for silver spheres of diameters 20 nm (solid line), 60 nm (long dashes), 120 nm (short dashes), 240 nm (dot dashes) and 300 nm (medium dashes) in air. The 120-nm diameter sphere exhibits a broad dipole resonance at ~430 nm and a narrower quadrupole resonance at ~355 nm. (*Mathematica* simulation)

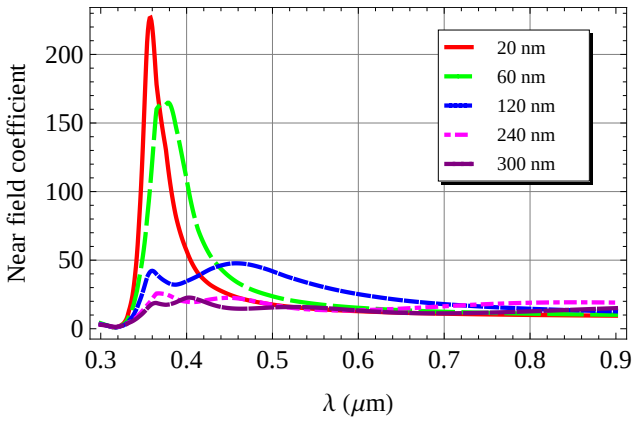

Fig. 9.8. Extinction coefficient as a function of wavelength, λ, for silver spheres of diameters 20 nm (solid line), 60 nm (long dashes), 120 nm (short dashes), 240 nm (dot dashes) and 300 nm (medium dashes) in air. The 120-nm diameter sphere exhibits a broad dipole resonance at ~430 nm and a narrower quadrupole resonance at ~355 nm. (*Mathematica* simulation)

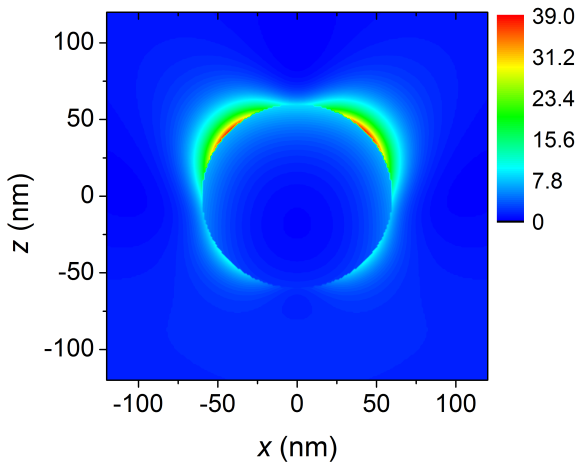

Fig. 9.9. The field intensity, $|E|^2$, in the vicinity of a 120 nm silver sphere in air at the quadrupole resonance wavelength of 360 nm when excited by a plane wave of unit amplitude traveling in the -*z*-direction and polarized along the *x*-direction. The refractive index of silver is $0.196 + 1.533i$ at this wavelength.

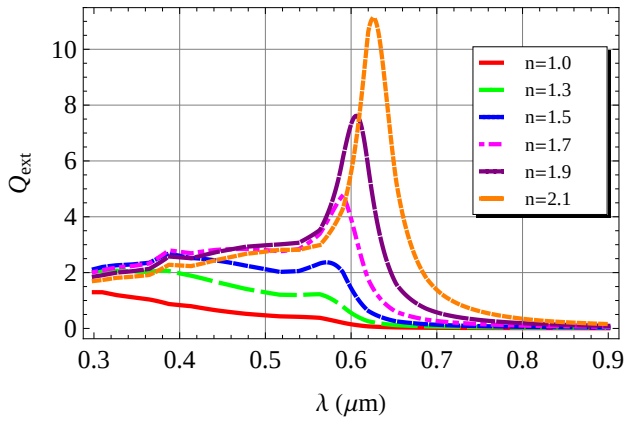

Fig. 9.10. Extinction coefficient as a function of wavelength, λ, for copper spheres embedded in dielectrics with indices of refraction of 1.0 (solid line), 1.3 (long dashes), 1.5 (short dashes), 1.7 (dot dashes), 1.9 (medium dashes) and 2.1 (dots). (Mathematica simulation)

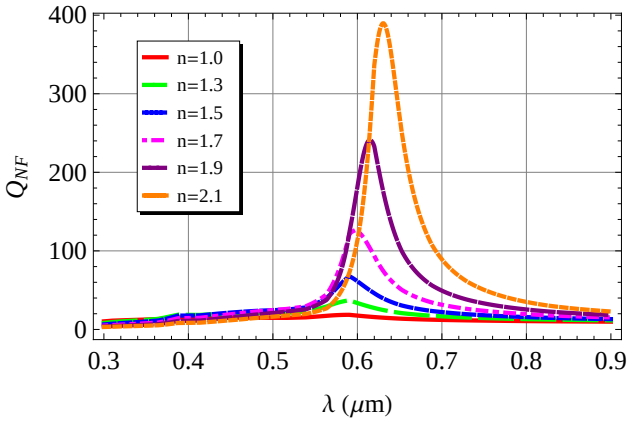

Fig. 9.11. Near field scattering coefficient as a function of wavelength, λ, for copper spheres embedded in dielectrics with indices of refraction of 1.0 (solid line), 1.3 (long dashes), 1.5 (short dashes), 1.7 (dot dashes), 1.9 (medium dashes) and 2.1 (dots). (Mathematica simulation)

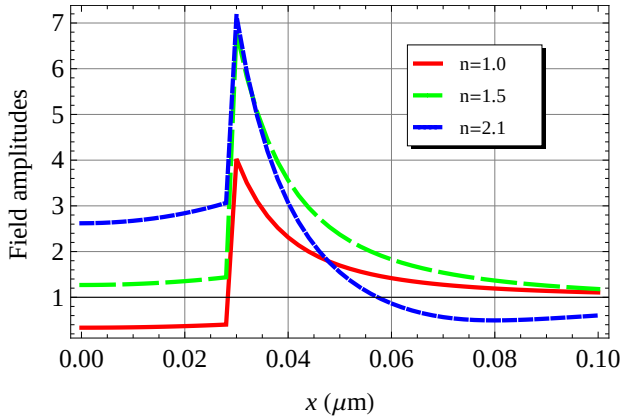

Fig. 9.12. Field along the *x*-direction excited by a plane wave incident upon a 60-nm copper sphere centered at the origin at a wavelength of 623 nm for refractive indices of the surrounding medium of 1.0 (solid), 1.5 (long dashes) and 2.1 (short dashes). (*Mathematica* simulation)

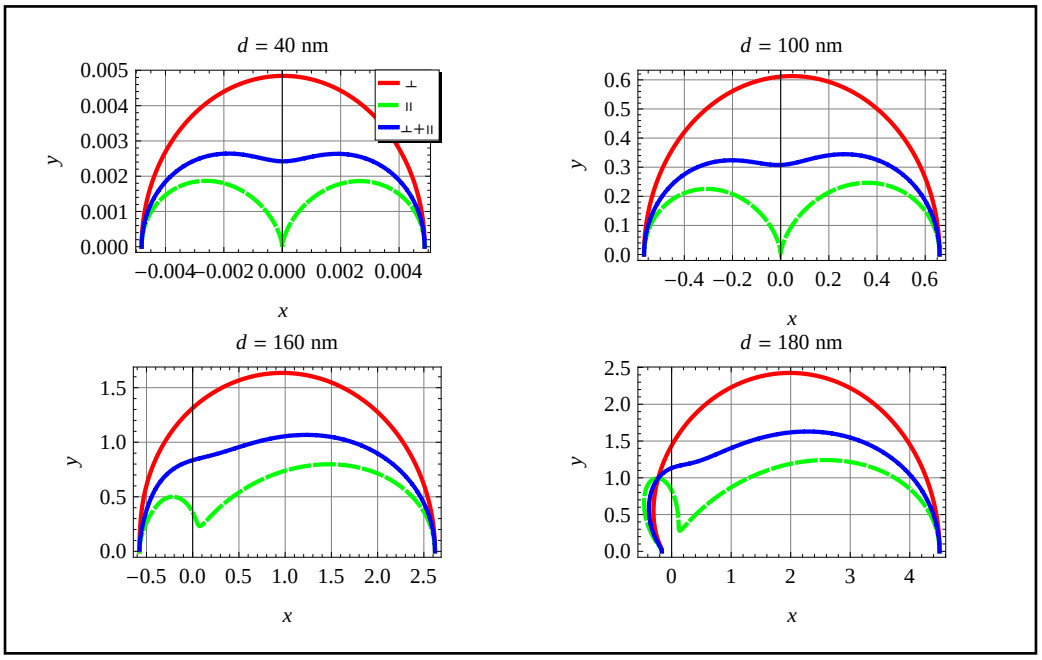

Fig. 9.13. Scattering diagrams for gold spheres of various diameters in water at a wavelength of 550 nm. The scattering pattern for light is shown for the plane through the center of the sphere which contains the incident wave vector and that is either perpendicular (solid line) or parallel to (dashed) the incident polarization, as well as the average of these two patterns (dotted). (*Mathematica* simulation)

9.1.3 Quasistatic approximation

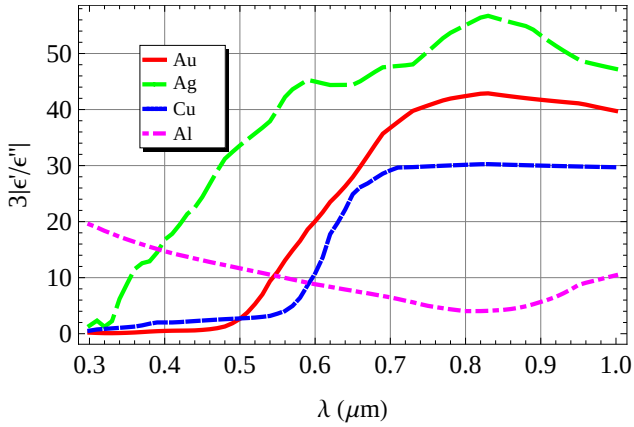

Fig. 9.14. Plot of the field enhancement factor, $3|\epsilon'/\epsilon''|$, as a function of wavelength, λ, for gold (solid line), silver (long dashes), copper (short dashes) and aluminum (dot dashes). (*Mathematica* simulation)

9.1.4 Ellipsoidal particles

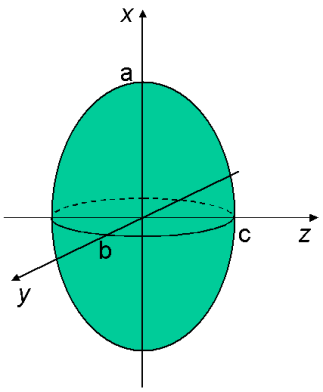

Fig. 9.15. Ellipsoidal particle with axes dimensions 2a, 2b, and 2c.

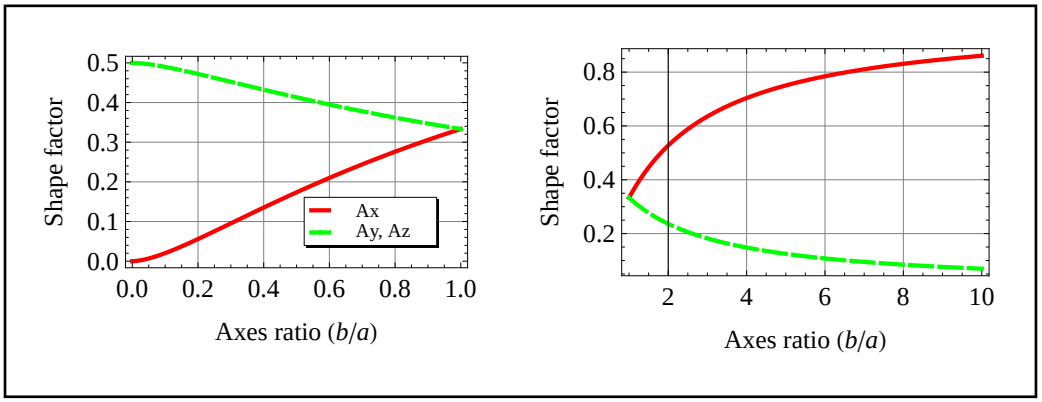

Fig. 9.16. Shape factors for (left) prolate spheroidal particles with the minor axes, *y* and *z*, equal in length, and (right) oblate spheroidal particles with major axes, *y* and *z*, equal in length. (*Mathematica* simulation)

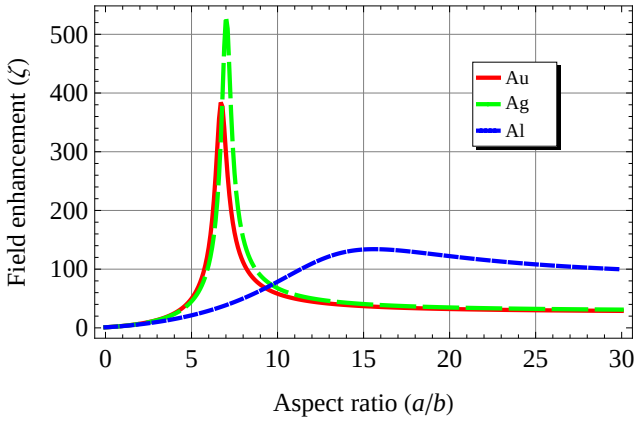

Fig. 9.17. The field enhancement factor for a spheroid, ζ, is computed as a function of the aspect ratio at a wavelength of 800 nm for gold (solid line), silver (long dashes) and aluminum (short dashes). (*Mathematica* simulation)

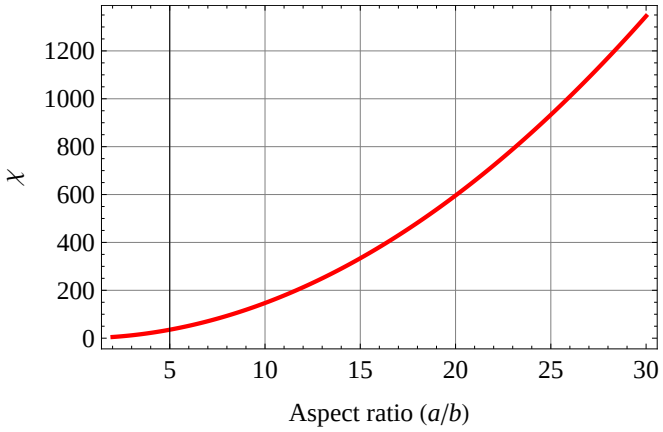

Fig. 9.18. The geometric field enhancement factor, χ, demonstrating the lightning rod effect for a prolate spheroid, is plotted as a function of the aspect ratio. (*Mathematica* simulation)

9.1.5 Localized surface plasmon damping

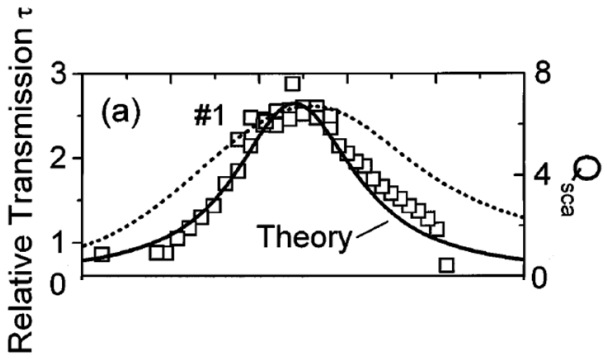

Fig. 9.19. The squares are the experimental transmission efficiency for a single 20 nm gold particle in TiO_2. The dotted line is the far field optical density for the composite film (arbitrary units). The solid line is the scattering efficiency from Mie theory. Reprinted with permission from T. Klar, M. Perner, S. Grosse, G. von Plessen, W. Spirkl, and J. Feldmann. *Phys. Rev. Lett.* **80** 4249 (1998) . © 1998 by the American Physical Society. [24]

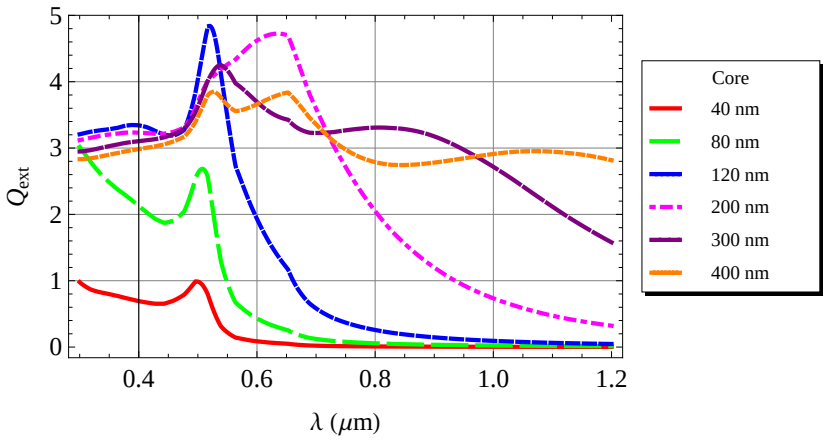

Fig. 9.20. Extinction coefficient of a Au NP in air as a function of wavelength, λ, for particle diameters of 40 nm (solid), 80 nm (long dashes), 120 nm (short dashes), 200 nm (dot dashes), 300 nm (medium dashes) and 400 nm (dots). (*Mathematica* simulation)

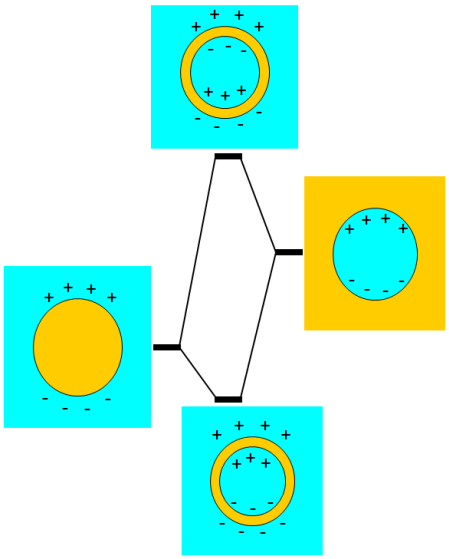

Fig. 9.21. Hybridization diagram exhibiting the SP modes of a nanosphere and nanovoid which interact in a nanoshell to produce two new modes at a higher and lower energy. From E. Prodan *et al.*, *Science* **302** (2003) 419. Reprinted with permission from AAAS. [42]

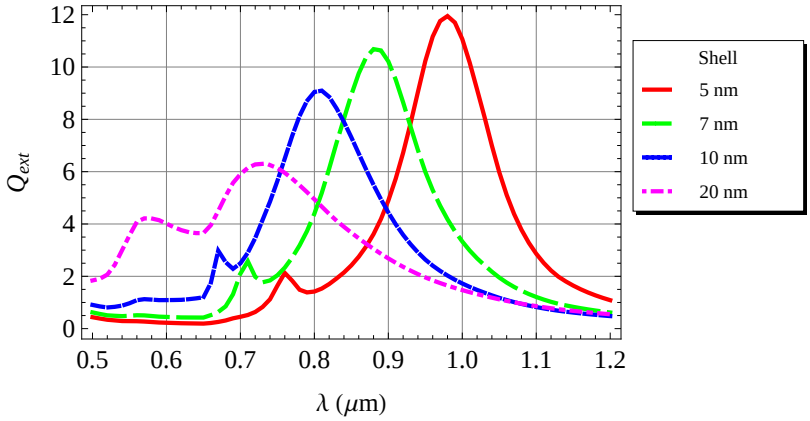

Fig. 9.22. Extinction coefficient, Q_{ext}, for a Au nanoshell surrounding a 120-nm silica core immersed in water for shell thicknesses of 5 nm (solid line), 7 nm (long dashes), 10 nm (short dashes) and 20 nm (dot dashes) as a function of wavelength, λ. (*Mathematica* simulation)

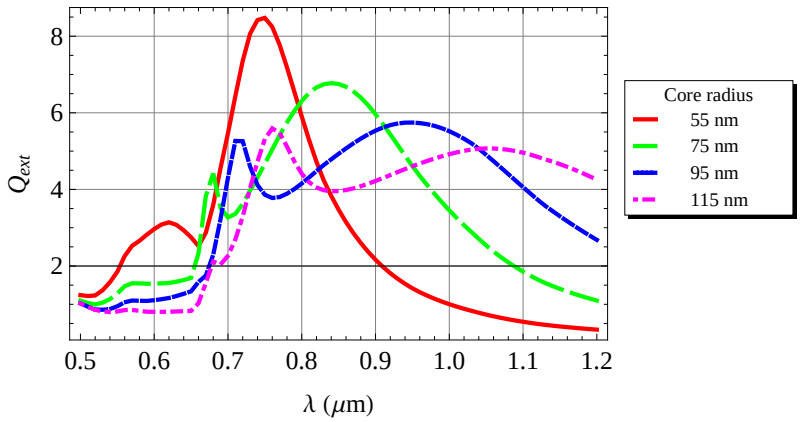

Fig. 9.23. Extinction coefficient, Q_{ext}, for a 13-nm Au nanoshell surrounding a silica core immersed in water for core thicknesses of 55 nm (solid line), 75 nm (long dashes), 95 nm (short dashes) and 115 nm (dot dashes) as a function of wavelength, λ. (*Mathematica* simulation)

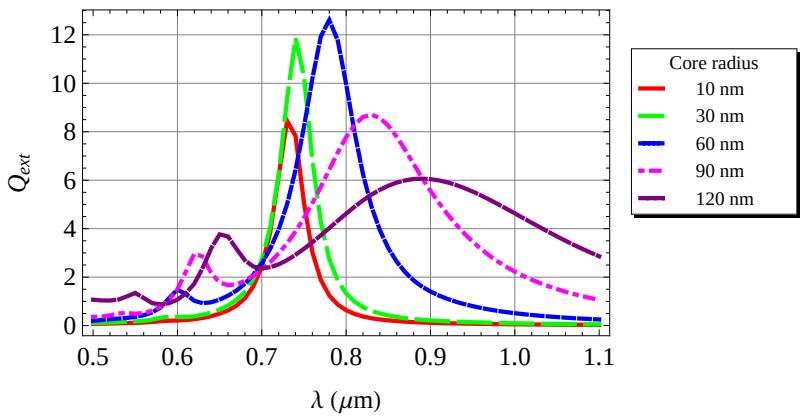

Fig. 9.24. Extinction coefficient, Q_{ext}, for Ag nanoshells of radii 10 nm (solid), 30 nm (long dashes), 60 nm (short dashes), 90 nm (dot dashes) and 120 nm (medium dashes) in vacuum with fixed ratio of 1.1 of the shell-to-core radii as a function of wavelength, λ. (*Mathematica* simulation)

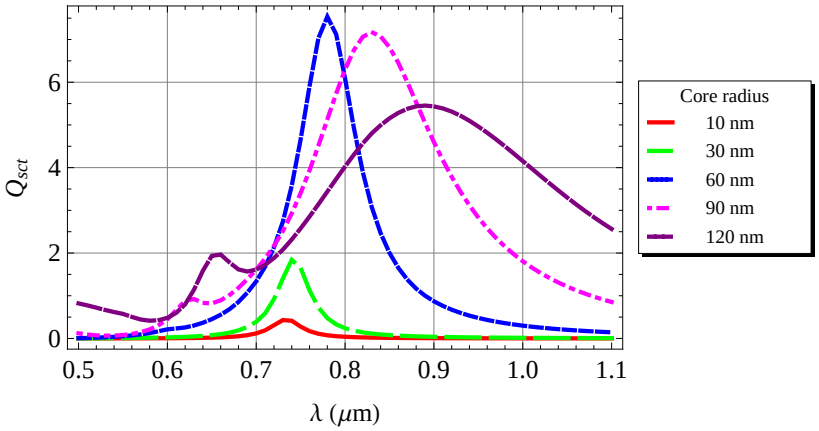

Fig. 9.25. Scattering coefficient, Q_{sct}, for Ag nanoshells of radii 10 nm (solid line), 30 nm (long dashes), 60 nm (short dashes), 90 nm (dot dashes) and 120 nm (medium dashes) in vacuum with fixed ratio of 1.1 of the shell-to-core radii as a function of wavelength, λ. (*Mathematica* simulation)

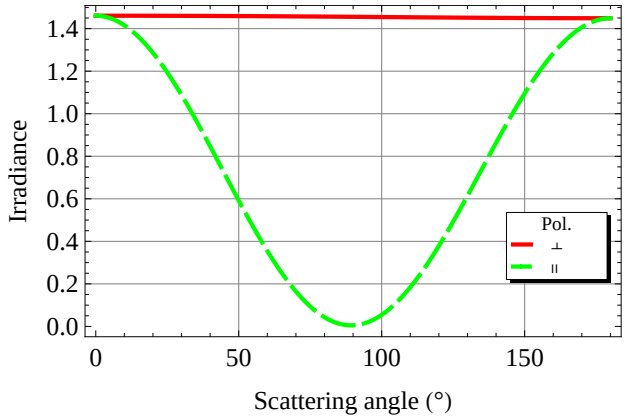

Fig. 9.26. Dipole scattering diagram for a gold nanoshell with an 11 nm thickness on a silica core with a radius of 60 nm in water at a wavelength of 830 nm. The scattered irradiance is shown as a function of scattering angle for the plane of the incident wavevector that is perpendicular to the incident polarization vector (solid line), and that contains the incident polarization vector (dashes). (*Mathematica* simulation)

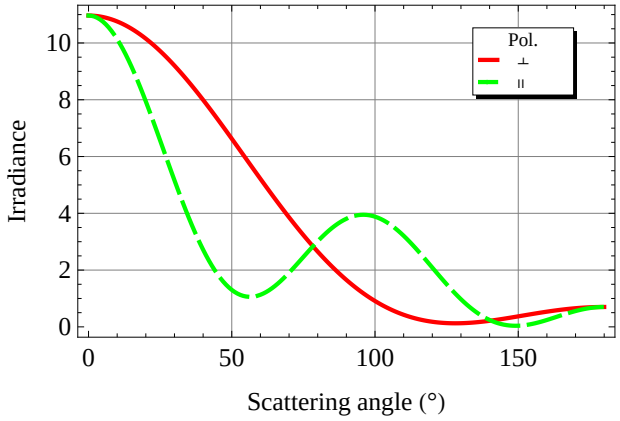

Fig. 9.27. Quadrupole scattering diagram for a gold nanoshell with a 15 nm thickness on a silica core with a radius of 135 nm in water at a wavelength of 800 nm. The scattered irradiance is shown as a function of scattering angle for the plane of the incident wavevector that is perpendicular to the incident polarization vector (solid line), and that contains the incident polarization vector (dashes). (*Mathematica* simulation)

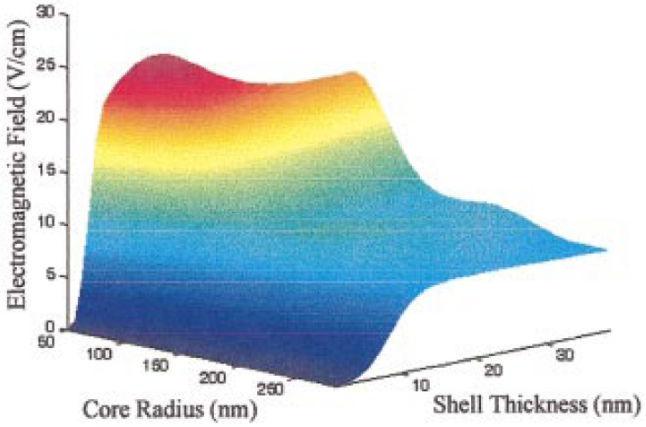

Fig. 9.28. Magnitude of the electric field at the surface of a silver nanoshell on a silica core as a function of core radius and shell thickness at a wavelength of 1064 nm. Reprinted with permission from J. B. Jackson, S. L. Westcott, L. R. Hirsch, J. L. West and N. J. Halas. *Appl. Phys. Lett.* **82** #2, 257 (2003). Copyright 2003, American Institute of Physics. [34]

9.4 Other nanoparticle shapes

9.4.1 Nanodisks

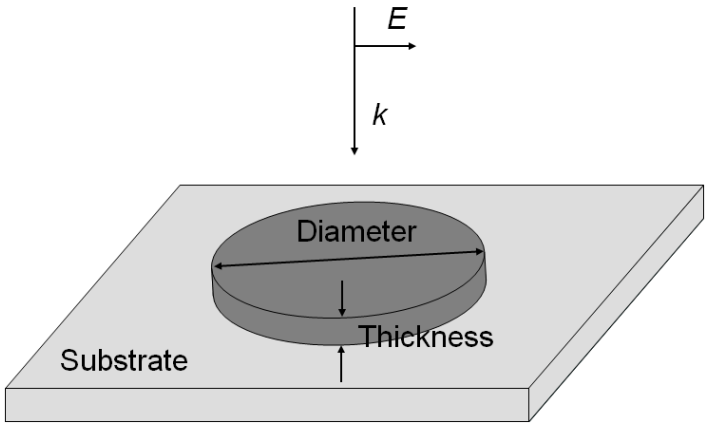

Fig. 9.29. Geometry of the gold disks and the incident plane wave with an electric field, *E*, and wavevector, *k*, in the FDTD simulations.

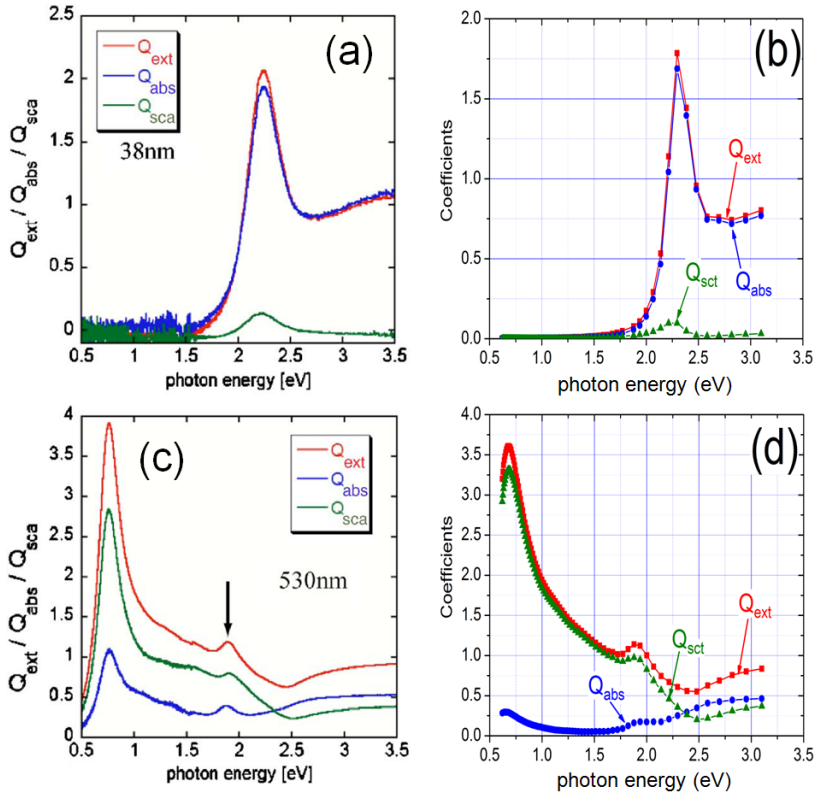

Fig. 9.30. Comparison of (left) experiment and (right) FDTD simulation for extinction, absorption, and scattering efficiencies of 20 nm thick gold nanodisks on a substrate of glass in air with diameters of (a) and (b) 38 nm, and (c) and (d) 530 nm. There are no adjustable parameters in the FDTD simulations. (a) and (c) reprinted with permission from C. Langhammer, B. Kasemo and I. Zoric. *J. Chem. Phys.* **126** 194702 (2007), © 2007 American Institute of Physics. [62]

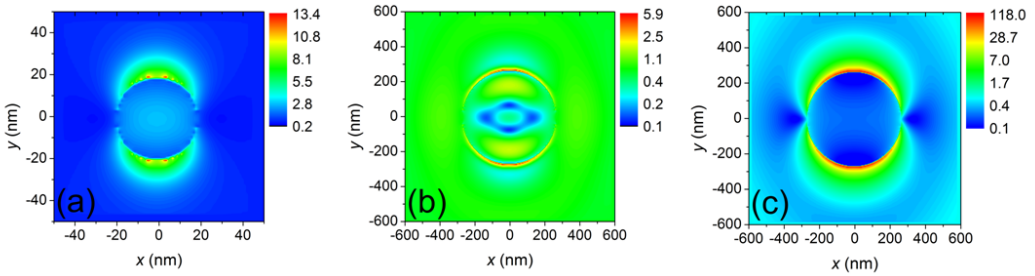

Fig. 9.31. Near field intensity for 20 nm thick gold nanodisks on a substrate of glass in air with (a) a diameters of 38 nm and a frequency of 2.25 eV, (b) a diameter of 530 nm and a frequency of 1.9 eV, and (c) a diameter of 530 nm and a frequency of 0.67 eV. The FDTD cell size is $(2\text{ nm})^3$ for the smaller disk and $(4.0 \times 2.5 \times 4.0)\text{ nm}^3$ for the larger disk.

9.4.2 Nanorods

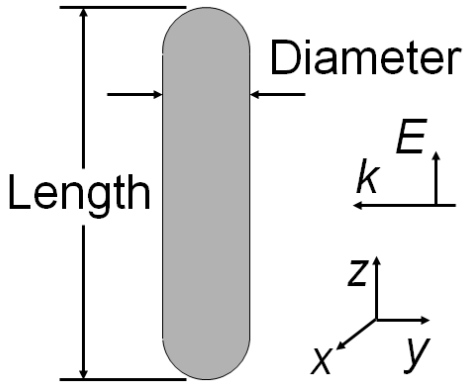

Fig. 9.32. Geometry of nanorods for FDTD simulations.

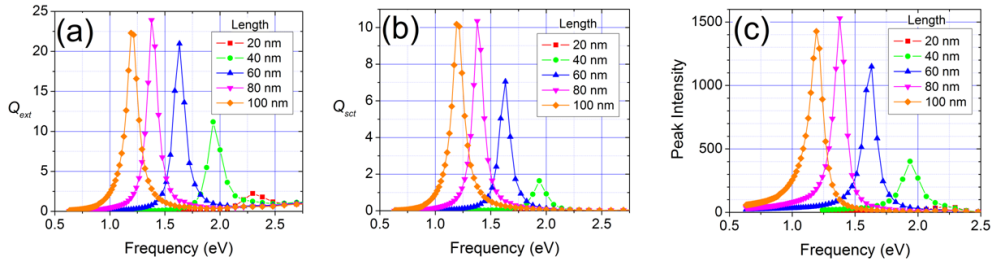

Fig. 9.33. (a) Extinction, and (b) scattering coefficients, and (c) peak field intensity for gold nanorods of 20 nm diameter and various lengths as a function of frequency in a medium with index 1.5. The peak scattering coefficient for the 20 nm nanorods occurs at a frequency of 2.3 eV but is only 0.042 and so does not show up on this scale. (FDTD simulations)

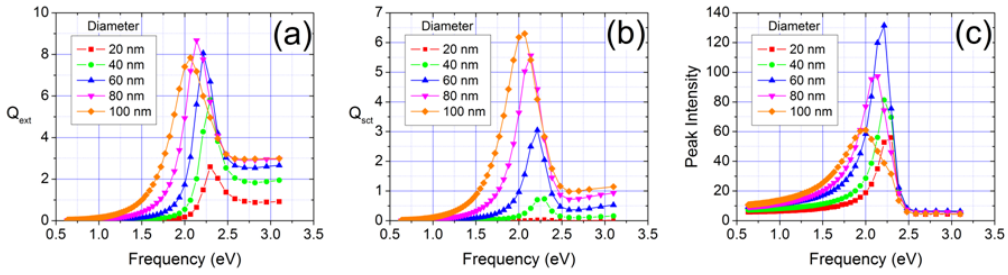

Fig. 9.34. (a) Extinction and (b) scattering coefficients, and (c) peak field intensity for gold spheres of various diameters as a function of frequency in a medium with index 1.5. (FDTD simulations)

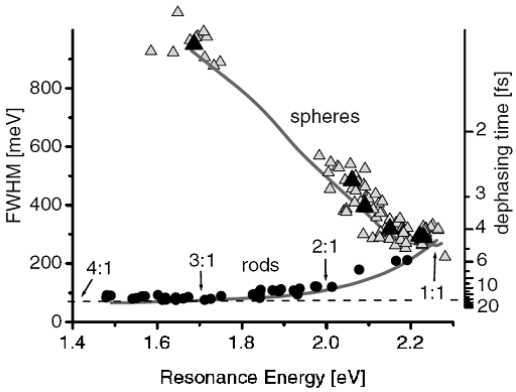

Fig. 9.35. Experimental measurements of the full width at half maximum linewidth of the LSPR for gold nanorods of various aspect ratios and spheres of various diameters. Reprinted with permission from C. Sönnichsen, T. Franzl, T. Wilk, G. von Plessen, J. Feldmann, O. Wilson and P. Mulvaney. *Phys. Rev. Lett.* **88** 077402 (2002). © 2002 by the American Physical Society. [25]

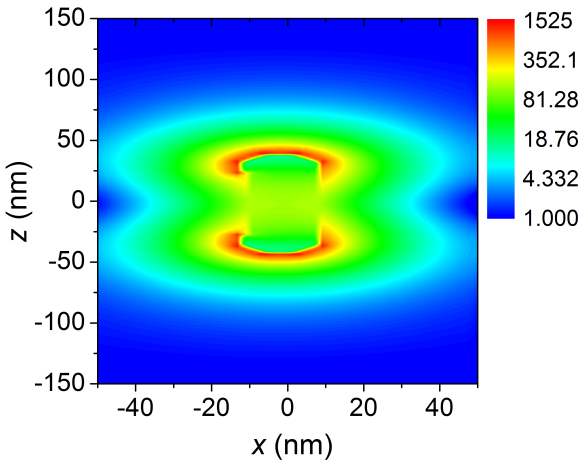

Fig. 9.36. $|E|^2$ field intensity in the vicinity of a gold nanorod with a diameter of 20 nm and a length of 80 nm, embedded in a dielectric with index 1.5, and at a frequency of 1.38 eV (λ = 900 nm). (FDTD simulations)

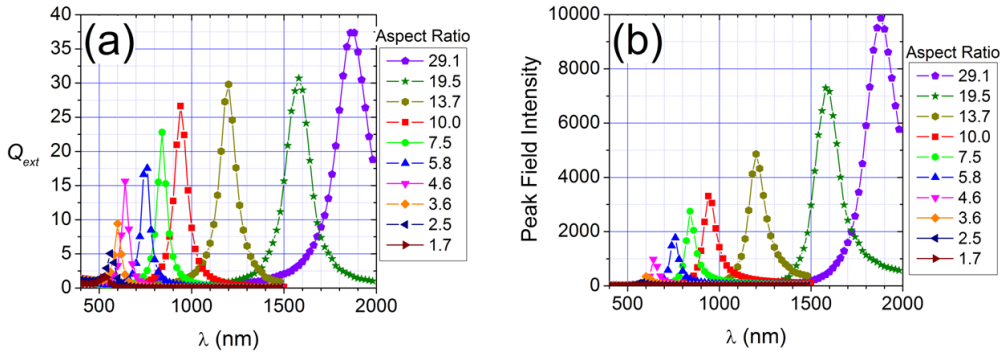

Fig. 9.37. (a) Q_{ext} and (b) peak $|E|^2$ field intensity for gold nanorods with a volume of 7900 $nm^3$for several different aspect ratios as a function of wavelength, λ. The length of the rod varies from 100 nm to 30 nm, while the diameter of the rod varies from 10 nm to 18 nm. The surrounding dielectric is air. (FDTD simulations)

9.4.3 Nanotriangles

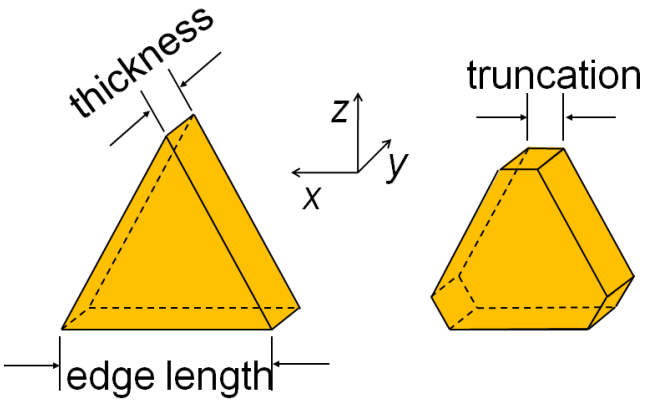

Fig. 9.38. Dimensions used for modeling triangular nanoparticles.

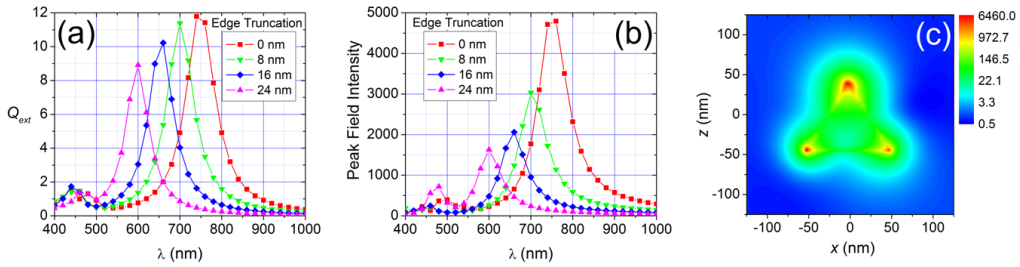

Fig. 9.39. (a) Extinction spectra for equilateral silver triangles in water with edge length of 100 nm, thickness of 16 nm, and three different edge truncations, and (b) peak field intensity within the water. (c) Field intensity contours for the untruncated triangle at a wavelength of 780 nm. The incident plane wave is polarized along the *z*-direction. (FDTDsimulations)

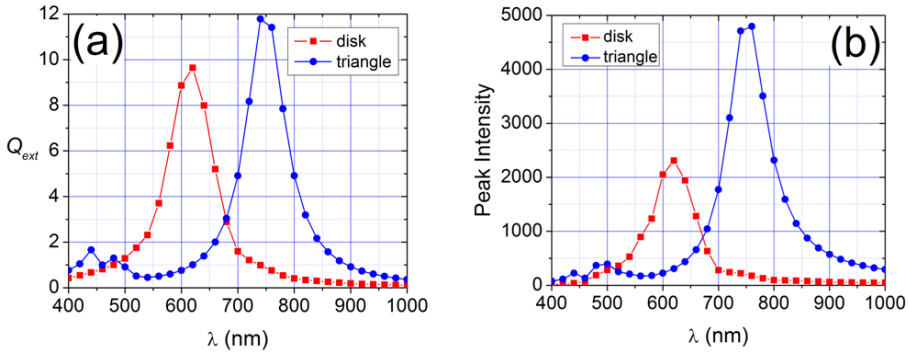

Fig. 9.40. (a) Extinction efficiency and (b) peak field intensity comparison of a 75 nm diameter silver disk and an equilateral silver triangle with a 100 nm edge length, both 16 nm-thick and surrounded by water as a function of wavelength, λ. (FDTD simulation)

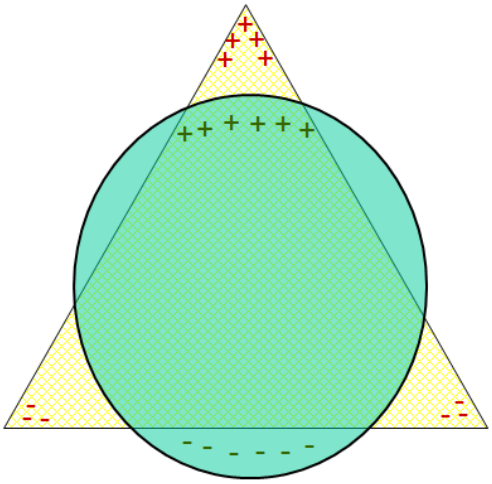

Fig. 9.41. Comparison of surface charge density for triangles and disks of identical cross section. The greater separation of surface charge for the triangular NP leads to a longer resonant wavelength.

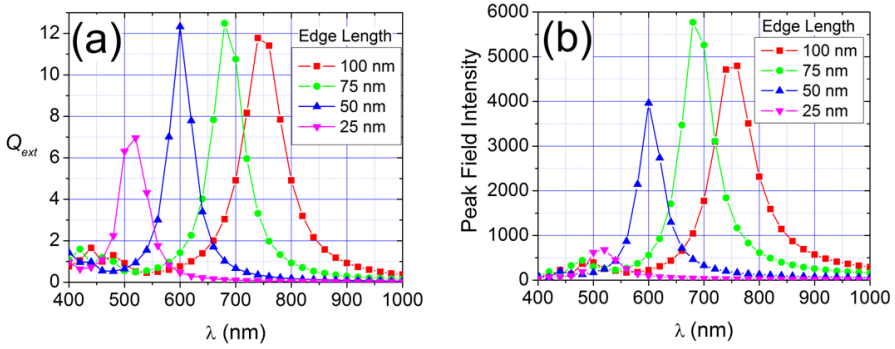

Fig. 9.42. (a) Extinction coefficient, Q_{ext}, and (b) peak field intensity as a function of wavelength, λ, for several different edge lengths of an equilateral silver triangle NP with a thickness of 16 nm in water. (FDTD simulation)

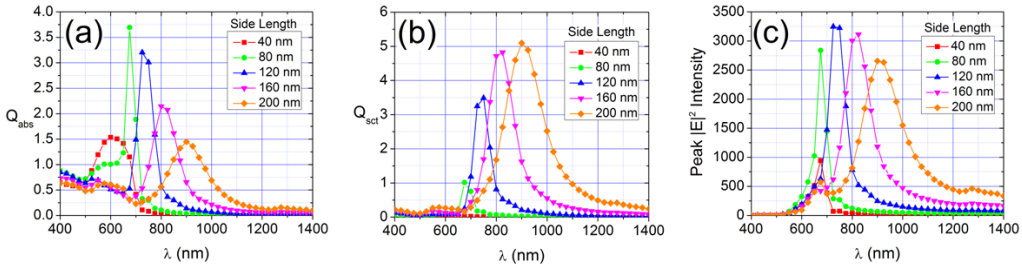

Fig. 9.43. (a) Absorption coefficient, Q_{abs}, (b) scattering coefficient , Q_{sct}, and (c) peak electric field intensity for 20 nm thick, equilateral gold triangles on a glass substrate in air as a function of wavelength, λ. (FDTD simulations)

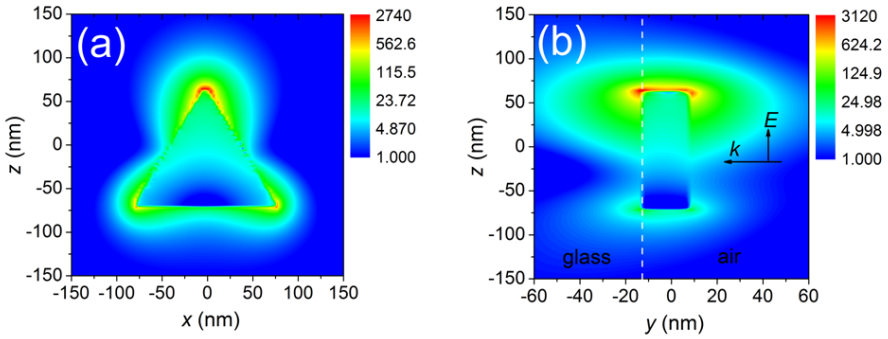

Fig. 9.44. (a) Near field intensity for a gold triangle with a 160 nm side length at a wavelength of 825 nm through the plane of the triangle at the air-glass interface, and (b) near field intensity through the center of the triangle at $x = 0$. The dashed line indicates the air-glass interface. The incident plane wave is polarized in the vertical direction. (FDTD simulations)

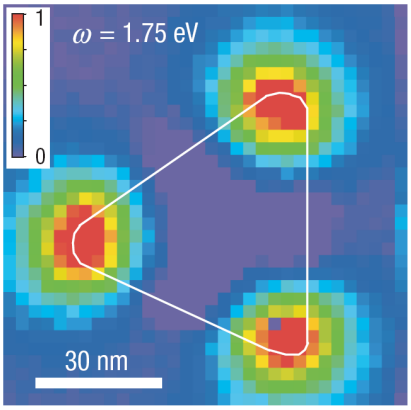

Fig. 9.45. Intensity map of the electron beam at an energy loss of 1.75 eV as it is rastered across a silver triangle NP on a mica substrate with an edge length of ~78 nm. Reprinted by permission from Macmillan Publishers Ltd: *Nat. Phys.* © 2007. [72]

9.5 Dual nanoparticles

9.5.1 Dual nanodisks

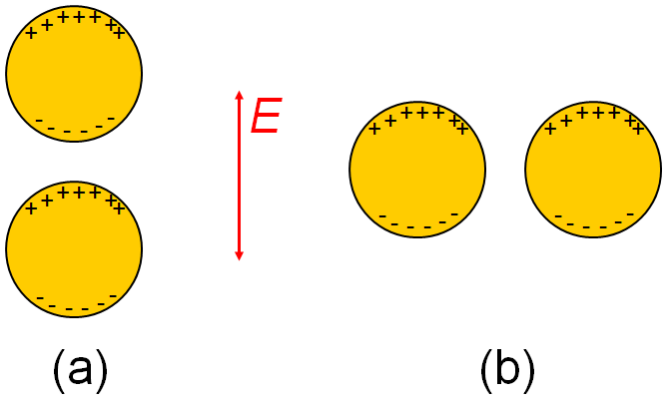

Fig. 9.46. Surface charge diagram for dual nanodisks excited by an incident field with the indicated polarization.

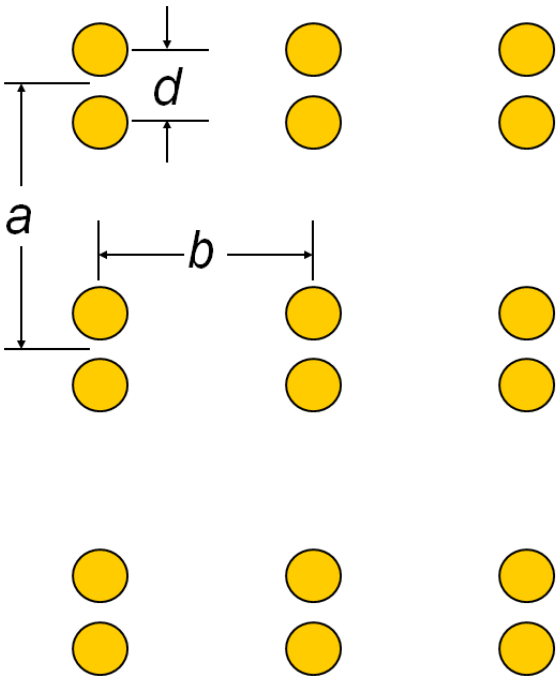

Fig. 9.47. Geometry of dual gold disk array where the disk diameter is 150 nm. The period "*a*" between rows is 900 nm. The period "*b*" between columns is 450 nm. There are three different samples with center-to-center spacing "*d*" between disks of 150, 300, and 450 nm, respectively. The former sample corresponds to the disks just touching. The latter sample corresponds to a square lattice of disks.

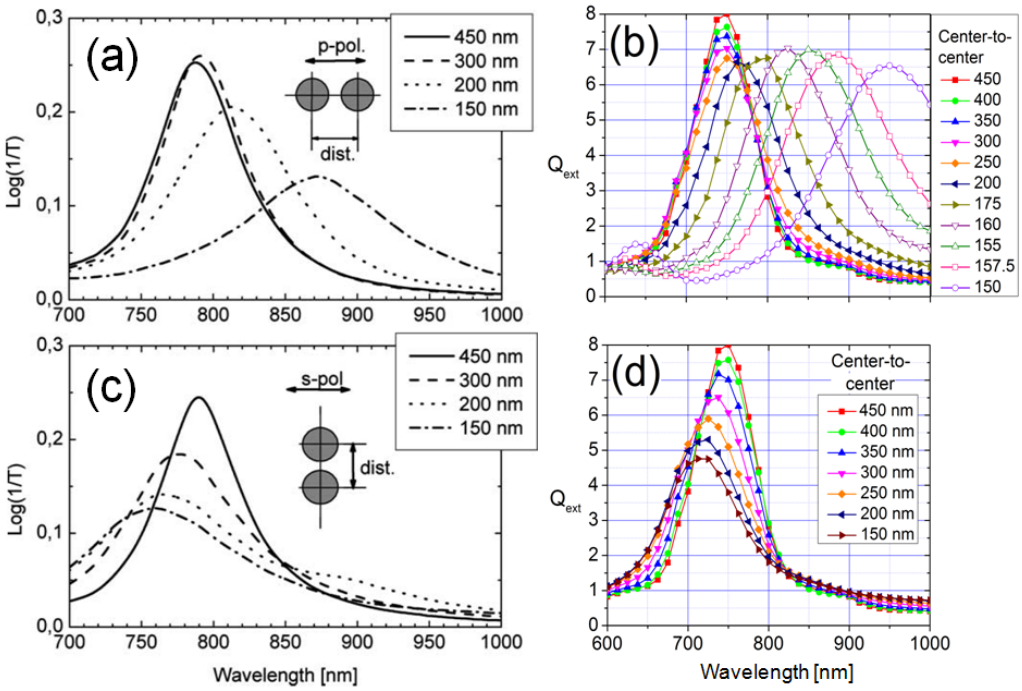

Fig. 9.48. Comparison of the (a,c) experimental, and (b,d) FDTD simulated values for the extinction coefficient of dual gold disk arrays for incident light polarized (a,b) parallel to, and (c,d) perpendicular to the dual disk axis. Figs. (a) and (c) reprinted from *Opt. Commun.*, **220** /1-3, W. Rechberger, A. Hohenau, A. Leitner, J. R. Krenn, B. Lambrecht, and F. R. Aussenegg, "Optical properties of two interacting gold nanoparticles," (2003) 137, © 2003, with permission from Elsevier.

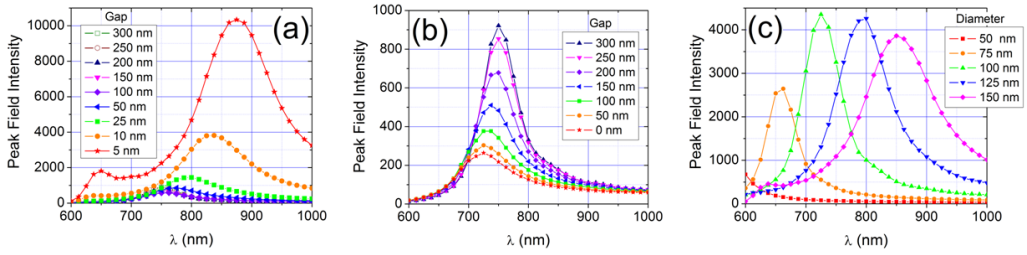

Fig. 9.49. Theoretical values for the peak field intensity of dual gold disk arrays for incident light polarized (a) parallel to and (b) perpendicular to the dual disk axis as a function of gap between the disks. (c) Theoretical values for the peak field intensity for dual gold disks with a 10 nm gap and various disk diameters. (FDTD simulations)

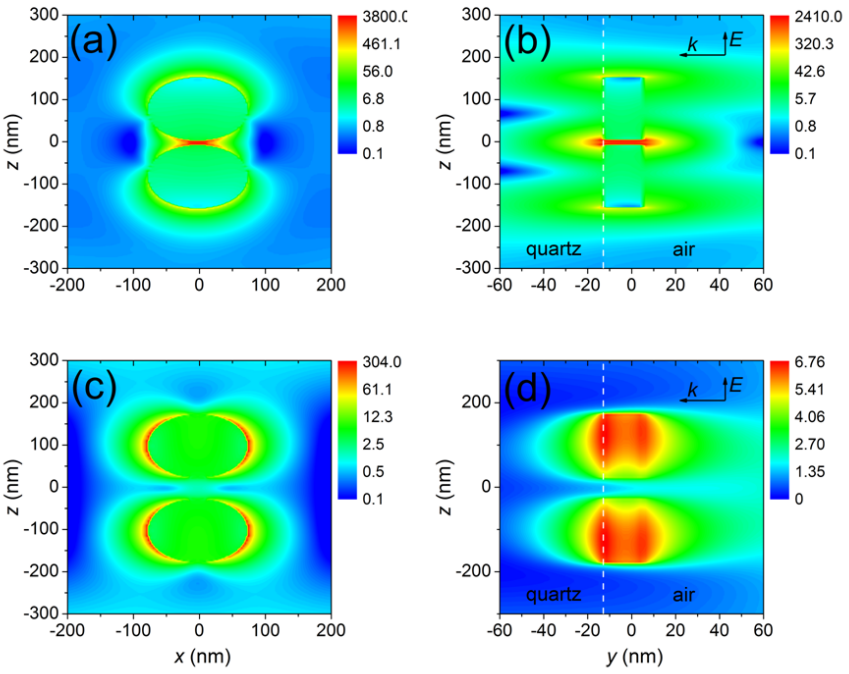

Fig. 9.50. Field intensity around a pair of gold disks with a 150 nm diameter, 17.5 nm thickness and 10 nm gap on a quartz substrate and surrounded by air at a wavelength of 825 nm. In (a) and (b) the incident light is polarized parallel to the axis connecting the disks. In (c) and (d) the incident light is poalrized perpendicular to this axis. (FDTD simulations)

9.5.2 Bow ties

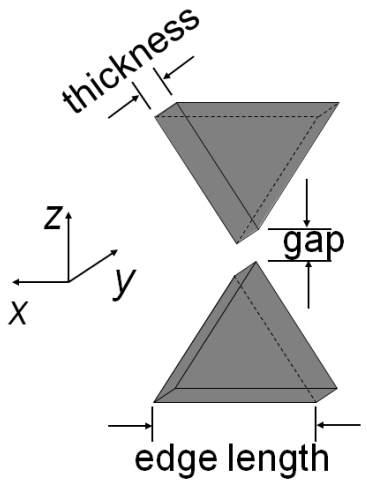

Fig. 9.51. Dimensions of the bow tie NPs.

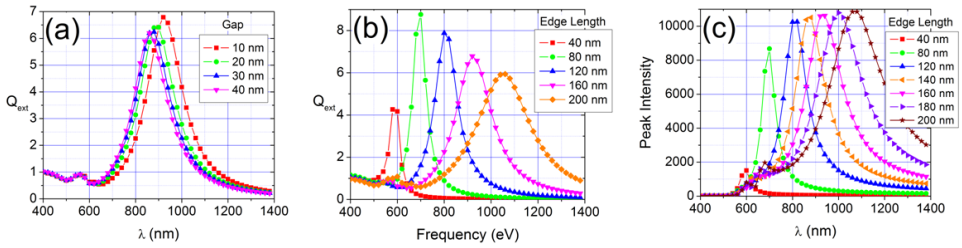

Fig. 9.52. (a) Extinction coefficient, Q_{ext}, (b) scattering coefficient, Q_{sct}, and (c) peak electric field intensity for gold bow tie NPs on a glass substrate that are 20 nm thick with various edge lengths and surrounded by air. (FDTD simulations)

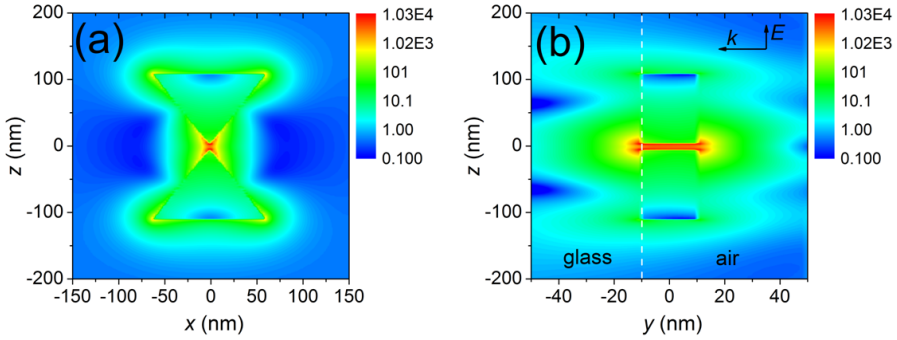

Fig. 9.53. Electric field intensity (a) in the plane and (b) through a cross section at x = 0 of a gold bow tie nanoantenna with an edge length of 120 nm, a thickness of 20 nm, and a gap of 10 nm at its resonant wavelength of 820 nm. (FDTD simulations)

Exercises

1. In the introduction of this chapter, it was asserted that silver nanoparticles embedded in glass impart a yellow color while gold particles impart a red color. Compute the extinction coefficient for 50 nm spherical silver and gold particles in a medium with a refractive index of 1.5 to see if this statement makes sense. Note: the wavelength range of yellow light is ~580-600 nm, and of red light is ~620-780 nm.

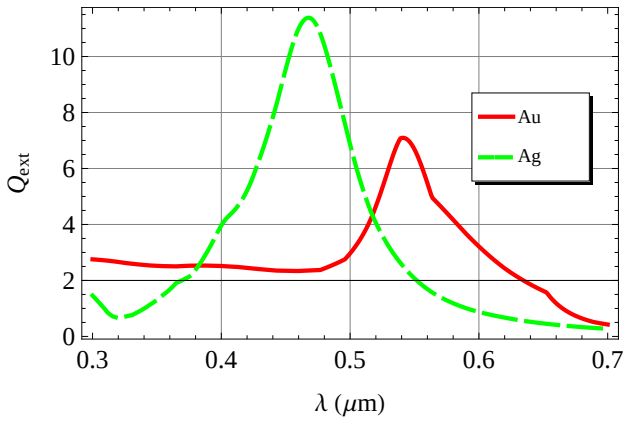

2. For gold nanoshells on a silica core in vacuum, let the outer shell radius be 10% larger than the core radius. As the core radius is varied from 20 nm to 120 nm what is the maximum extinction coefficient? How does this compare to silver (see Fig. 9.24)?

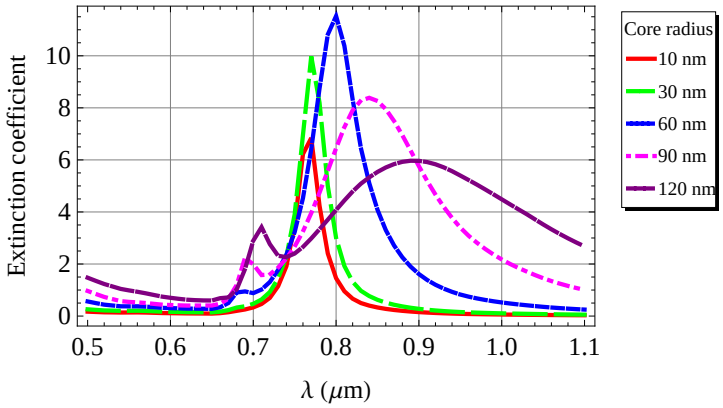

References

1. A. D. McFarland and R. P. Van Duyne. Single silver nanoparticles as real-time optical sensors with zeptomole sensitivity. *Nano Lett.* **3** (2003) 1057.

2. M. Moskovits. Surface-enhanced spectroscopy. *Rev. Mod. Phys.* **57** (1985) 783.

3. R. Elghanian, J. J. Storhoff, R. C. Mucic, R. L. Letsinger and C. A. Mirkin. Selective colorimetric detection of polynucleotides based on the distance-dependent optical properties of gold nanoparticles. *Science* **277** (1997) 1078.

4. X. Huang, I. H. El-Sayed, W. Qian, and M. A. El-Sayed. Cancer cell imaging and photothermal therapy in the near-infrared region by using gold nanorods. *J. Am. Chem Soc.* **128** (2006) 2115.

5. M. L. Brongersma, J. W. Hartman, and H. A. Atwater. Electromagnetic energy transfer and switching in nanoparticle chain arrays below the diffraction limit. *Phys. Rev. B* **62** (2000) R16356.

6. D. Ricard, P. Roussignol and C. Flytzanis. Surface-mediated enhancement of optical phase conjugation in metal colloids. *Opt. Lett.* **10** (1985) 511.

7. L. Novotny, R. X. Bian, and X. S. Xie. Theory of nanometric optical tweezers. *Phys. Rev. Lett.* **79** (1997) 645.

8. J. Aizprurua, P. Hanarp, D. S. Sutherland, M. Käll, G. W. Bryant, and F. J. García de Abajo. Optical properties of gold nanorings. *Phys. Rev. Lett.* **90** (2003) 057401.

9. K. -H. Su, Q. -H. Wei, X. Zhang, J. J. Mock, D. R. Smith, and S. Schultz. Interparticle coupling effects on plasmon resonances of nanogold particles. *Nano Lett.* **3** (2003) 1087.

10. H. Xu and M. Käll. Surface-plasmon-enhanced optical forces in silver nanoaggregates. *Phys. Rev. Lett.* **89** (2002) 246802.

11. G. Mie. Beiträge zur optik trüber medien, speziell kolloidaler metallösungen. *Ann. d. Physik* **25** (1908) 377.

12. C. F. Bohren and D. R. Huffman. *Absorption and Scattering of Light by Small Particles* (New York: John Wiley, 1983) chap. 4.

13. B. J. Messinger, K. U. von Raben, R. K. Chang and P. W. Barber. Local fields at the surface of noble-metal microspheres. *Phys. Rev. B* **24** (1981) 649.

14. P. B. Johnson and R. W. Christy. Optical constants of copper and nickel as a function of temperature. *Phys. Rev. B* **11** (1975) 1315.

15. U. Kreibig and M. Vollmer, *Optical Properties of Metal Clusters* (Berlin: Springer-Verlag, 1995) p. 125.

16. J. Δ. Jackson. *Classical Electrodynamics*, 2nd ed. (New York: John Wiley, 1975), p. 100.

17. P. F. Liao and A. Wokaun. Lightning rod effect in surface enhanced Raman scattering. *J. Chem Phys.* **76** (1982) 751.

18. B. Lamprecht, J. R. Krenn, A. Leitner, and F. R. Aussenegg. Resonant and off-resonant light-driven plasmons in metal nanoparticles studied by femtosecond-resolution third-harmonic generation. *Phys. Rev. Lett.* **83** (1999) 4421.

19. J. Lehmann, M. Merschdorf, W. Pfeiffer, A. Thon, S. Voll, and G. Gerber. Surface plasmon dynamics in silver nanoparticles studied by femtosecond time-resolved photoemission. *Phys. Rev. Lett.* **85** (2000) 2921.

20. T. Zentgraf, A. Christ, J. Kuhl and H. Giessen. Tailoring the ultrafast dephasing of quasiparticles in metallic photonic crystals. *Phys. Rev. Lett.* **93** (2004) 243901.

21. I. D. Mayergoyz, Z. Zhang, and G. Miano. Analysis of dynamics of excitation and dephasing of plasmon resonance modes in nanoparticles. *Phys. Rev. Lett.* **98** (2007) 147401.

22. U. Freibig and M. Vollmer, *ibid*, Sect. 2.2.2.

23. M. Perner, P. Bost, U. Lemmer, G. von Plessen, J. Feldmann, U. Becker, M. Mennig, M. Schmitt and H. Schmidt. Optically induced damping of the surface plasmon resonance in gold colloids. *Phys. Rev. Lett.* **78** (1997) 2192.

24. T. Klar, M. Perner, S. Grosse, G. von Plessen, W. Spirkl and J. Feldmann. Surface-plasmon resonances in single metallic nanoparticles. *Phys. Rev. Lett.* **80** (1998) 4249.

25. C. Sönnichsen, T. Franzl, T. Wilk, G. von Plessen, J. Feldmann, O. Wilson and P. Mulvaney. Drastic reduction of plasmon damping in gold nanorods. *Phys. Rev. Lett.* **88** (2002) 077402.

26. P. B. Johnson and R. W. Christy. Optical constants of the noble metals. *Phys. Rev. B* **6** (1972) 4370.

27. V. Pustovit and T. V. Shahbazyan. Finite-size effects in surface-enhanced Raman scattering in noble-metal nanoparticles: a semiclassical approach. *J. Opt. Soc. Am. A* **23** (2006) 1369.

28. R. M. Cole, J. J. Baumberg, F. J. Garcia de Abajo, S. Mahajan, M. Abdelsalam and P. N. Bartlett. Understanding plasmons in nanoscale voids. *Nano Lett.* **7** (2007) 2094.

29. S. P. Apell, P. M. Echenique and R. H. Ritchie. Sum rules for surface plasmon frequencies. *Ultramicrosc.* **65** (1996) 53.

30. A. E. Neeves and M. H. Birnboim. Composite structures for the enhancement of nonlinear-optical susceptibility. *J. Opt. Soc. Am. B* **6** (1989) 787.

31. S. J. Oldenburg, J. B. Jackson, S. L. Westcott and N. J. Halas. Infrared extinction properties of gold nanoshells. *Appl. Phys. Lett.* **75** (1999) 2897.

32. G. D. Hale, J. B. Jackson, O. E. Shmakova, T. R. Lee and N. J. Halas. Enhancing the active lifetime of luminescent semiconducting polymers via doping with metal nanoshells. *Appl. Phys. Lett.* **78** (2001) 1502.

33. S. J. Oldenburg, S. L. Westcott, R. D. Averitt, and N. J. Halas. Surface enhanced Raman scattering in the near infrared using metal nanoshell substrates. *J. Chem. Phys.* **111** (1999) 4729.

34. J. B. Jackson, S. L. Westcott, L. R. Hirsch, J. L. West and N. J. Halas. Controlling the surface enhanced Raman effect via the nanoshell geometry. *Appl. Phys. Lett.* **82** (2003) 257.

35. S. R. Sershen, S. L. Westcott, N. J. Halas and J. L. West. Temperature-sensitive

polymer-nanoshell composites for photothermally modulated drug delivery. *J. Biomed. Mater. Res.* **51** (2000) 293.

36. L. R. Hirsch, R. J. Stafford, J. A. Bankson, S. R. Sershen, B. Rivera, R. E. Price, J. D. Hazle, N. J. Halas and J. L. West. Nanoshell-mediated near-infrared thermal therapy of tumors under magnetic resonance guidance. *Proc. Natl. Acad. Sci. U.S.A.* **100** (2003) 13549.

37. R. D. Averitt, D. Sarkar and N. J. Halas. Plasmon resonance shifts of Au-coated Au_2S nanoshells: insight into multicomponent nanoparticle growth. *Phys. Rev. Lett.* **78** (1997) 4217.

38. S. J. Oldenburg, R. D. Averitt, S. L. Westcott and N. J. Halas. Nanoengineering of optical resonances. *Chem. Phys. Lett.* **288** (1998) 243.

39. S. Mohapatra, Y. K. Mishra, D. K. Avasthi, D. Kabiraji, J. Ghatak and S. Varma. Synthesis of gold-silicon core-shell nanoparticles with tunable localized surface plasmon resonance. *Appl. Phys. Lett.* **92** (2008) 103105.

40. A. B. R. Mayer, W. Gregner and R. J. Wannemacher. Preparation of silver-latex composites. *J. Phys. Chem B* **104** (2000) 7278.

41. J. B. Jackson and N. J. Halas. Silver nanoshells: variations in morphologies and optical properties. *J. Phys. Chem B* **105** (2001) 2743.

42. E. Prodan, C. Radloff, N. J. Halas and P. Nordlander. A hybridization model for the plasmon response of complex nanostructures. *Science* **302** (2003) 419.

43. C. Radloff and N. J. Halas. Plasmonic properties of concentric nanoshells. *Nano Lett.* **4** (2004) 1323.

44. H. Wang, F. Tam, N. K. Grady and N. J. Halas. Cu nanoshells: effects of interband transitions on the nanoparticle plasmon resonance. *J. Phys. Chem B* **109** (2005) 18218.

45. N. Halas. The optical properties of nanoshells. *Optics and Photonics News* (August, 2002) 26.

46. R. D. Averitt, S. L. Westcott and N. J. Halas. Linear optical properties of gold nanoshells. *J. Opt. Soc. Am. B* **16** (1999) 1824.

47. A. L. Aden and M. Kerker. Scattering of electromagnetic waves from two concentric spheres. *J. Appl. Phys.* **22** (1951) 1242.

48. T. Okamoto. Near-field spectral analysis of metallic beads. In *Near-field Optics and Surface Plasmon Polaritons* (Berlin: Springer, 2001) p. 112 ff.

49. S. L. Westcott, J. B. Jackson, C. Radloff and N. J. Halas. Relative contributions to the plasmon line shape of metal nanoshells. *Phys. Rev. B* **66** (2002) 155431.

50. G. Raschke, S. Brogl, A. S. Susha, A. L. Rogach, T. A. Klar, J. Feldmann, B. Fieres, N. Petkov, T. Bein, A. Nichtl and K. Kurzinger. Gold nanoshells improve single nanoparticle molecular sensors. *Nano Lett.* **4** (2004) 1853.

51. C. L. Nehl, N. K. Grady, G. P. Goodrich, F. Tam, N. J. Halas and J. H. Hafner. Scattering spectra of single gold nanoshells. *Nano Lett.* **4** (2004) 2355.

52. S. J. Oldenburg, G. D. Hale, J. B. Jackson and N. J. Halas. Light scattering from dipole and quadrupole nanoshell antennas. *Appl. Phys. Lett.* **75** (1999) 1063.

53. S. J. Norton and T. Vo-Dinh. Plasmon resonances of nanoshells of spheroidal shape. *IEEE Trans. Nanotechnol.* **6** (2007) 627.

54. S. R. Nicewarner-Peña, R. G. Freeman, B. D. Reiss, L. He, D. J. Peña, I. D. Walton, R. Cromer, C. D. Keating, and M. J. Natan. Submicrometer metallic barcodes. *Science* **294** (2001) 137.

55. C. Sönnichsen, T. Franzl, T. Wilk, G. von Plessen, J. Feldmann, O. Wilson and P. Mulvaney. Drastic reduction of plasmon damping in gold nanorods. *Phys. Rev. Lett.* **88** (2002) 077402.

56. G. Sando, A. D. Berry, P. M. Campbell, A. P. Baronavski and J. C. Owrutsky. Surface plasmon dynamics of high-aspect-ratio gold nanorods. *Plasmonics* **2** (2007) 23.

57. H. J. Huang, C. P. Yu, H. C. Chang, K. P. Chiu, H. M. Chen, R. S. Liu and D. P. Tsai. Plasmonic optical properties of a single gold nano-rod. *Opt. Exp.* **15** (2007) 7132.

58. S.-M. Lee, Y. Jun, S.-N. Cho and J. Cheon. Single-crystalline star-shaped nanocrystals and their evolution: programming the geometry of nano-building blocks. *J. Am. Chem. Soc.* **124** (2002) 11244.

59. C. L. Nehl, H. Liao and J. H. Hafner. Optical properties of star-shaped gold nanoparticles. *Nano Lett.* **6** (2006) 683.

60. C. Langhammer, Z. Yuan, I. Zoric and B. Kasemo. Plasmonic properties of supported Pt and Pd nanostructures. *Nano Lett.* **6** (2006) 833.

61. P. Hanarp, M. Kall anbd D. S. Sutherland. Optical properties of short range ordered arrays of gold disks prepared by colloidal lithography. *J. Phys. Chem. B* **107** (2003) 5768.

62. C. Langhammer, B. Kasemo and I. Zoric. Absorption and scattering of light by Pt, Pd, Ag, and Au nanodisks: absolute cross sections and branching ratios. *J. Chem. Phys.* **126** (2007) 194702.

63. C. Langhammer, M. Schwind, B. Kasemo and I. Zoric. Localized surface plasmon resonances in aluminum nanodisks. *Nano Lett.* **8** (2008) 1461.

64. J. Aizpurua, P. Hanarp, D. S. Sutherland, M. Kall, G. W. Bryant and F. J. Garcia de Abajo. Optical properties of gold nanorings. *Phys. Rev. Lett.* **90** (2003) 057401.

65. C. Aguirre, T. Kaspar, C. Radloff and N. J. Halas. CTAB mediated reshaping of metallodielectric nanoparticles. *Nano Lett.* **3** (2003) 1707.

66. H. Rochholz, N. Bocchio and M. Kreiter. Tuning resonances on crescent-shaped noble-metal nanoparticles. *New J. Phys.* **9** (2007) 53.

67. Y. Sun and Y. Xia. Shape-controlled synthesis of gold and silver nanoparticles. *Science* **298** (2002) 2176.

68. L. J. Sherry, S.-H. Chang, G. C. Schatz, R. P. Van Duyne, B. J. Wiley and Y. Xia. Localized surface plasmon resonance spectroscopy of single silver nanocubes. *Nano Lett.* **5** (2006) 2034.

69. C. L. Haynes and R. P. Van Duyne. Plasmon-sampled surface-enhanced Raman excitation spectroscopy. *J. Phys. Chem. B* **107** (2003) 7426.

70. A. J. Haes and R. P. Van Duyne. A nanoscale optical biosensor: sensitivity and selectivity of an approach based on the localized surface plasmon resonance spectroscopy of triangular silver nanoparticles. *J. Am. Chem. Soc.* **124** (2002) 10596.

71. G. S. Métraux, Y. C. Cao, R. Jin and C. A. Mirkin. Triangular nanoframes made of gold and silver. *Nano Lett.* **3** (2003) 519.

72. J. Nelayah, M. Kociak, O. Stéphan, F. J. G. de Abajo, M. Tencé, L. Henrard, D. Taverna, I. Pastoriza-Santos, L. M. Liz-Marzán and C. Colliex. Mapping surface plasmons on a single metallic nanoparticle. *Nat. Phys.* **3** (2007) 348.

73. L. J. Sherry, R. Jin, C. A. Mirkin, G. C. Schatz and R. P. Van Duyne. Localized surface plasmon resonance spectroscopy of single silver triangular nanoprisms. *Nano Lett.* **6** (2006) 2060.

74. K. L. Kelly, E. Coronado, L. L. Zhao and G. C. Schatz. The optical properties of metal nanoparticles: the influence of size, shape, and dielectric environment. *J. Phys. Chem. B* **107** (2003) 668.

75. J. C. Love, B. D. Gates, D. B. Wolfe, K. E. Paul and G. M. Whitesides. Fabrication and wetting properties of metallic half-shells with submicron diameters. *Nano Lett.* **2** (2002) 891.

76. M. Achermann, K. L. Shuford, G. C. Schatz, D. H. Dahanayaka, L. A. Bumm and V. I. Klimov. Near-field spectroscopy of surface plasmons in flat gold nanoparticles. *Opt. Lett.* **32** (2007) 2254.

77. A. K. Sheridan, A. W. Clark, A. Glidle, J. M. Cooper and D. R. S. Cumming. Multiple plasmon resonances from gold nanostructures. *Appl. Phys. Lett.* **90** (2007) 143105.

78. P. Hanarp, M. Käll, and D. S. Sutherland. Optical properties of short range ordered arrays of nanometer gold disks prepared by colloidal lithography. *J. Phys. Chem. B* **107** (2003) 5768.

79. C. Langhammer, Z. Yuan, I. Zoric, and B. Kasemo. Plasmonic properties of supported Pt and Pd nanostructures. *Nano Lett.* **6** (2006) 833.

80. H. Fredriksson, Y. Alaverdyan, A. Dmitriev, C. Langhammer, D. S. Sutherland, M. Zäch and B. Kasemo. Hole-mask colloidal lithograpy. *Adv. Mater.* **19** (2007) 4297.

81. T. Inagaki, K. Kagami, and E. T. Arakawa. Photoacoustic observation of nonradiative decay of surface plasmons in silver. *Phys. Rev. B* **24** (1981) 3644.

82. T. Inagaki, K. Kagami, and E. T. Arakawa. Photoacoustic study of surface plasmons in metals. *Appl. Opt.* **21** (1982) 949.

83. K. Sturm, W. Schülke, and J. R. Schmitz. Plasmon-Fano resonance inside the particle-hole excitation spectrum of simple metals and semiconductors. *Phys. Rev. Lett.* **68** (1992) 228.

84. M. van Exter and A. Lagendijk. Ultrashort surface-plasmon and phonon dynamics. *Phys. Rev. Lett.* **60** (1988) 49.

85. S.-S. Chang, C.-W. Shih, C.-D. Chen, W.-C. Lai, and C. R. C. Wang. The shape transition of gold nanorods. *Langmuir* **15** (1999) 701.

86. M. Pelton, M. Liu, K. C. Toussaint, Jr., H. Y. Kim, G. Smith, J. Pesic, P. Guyot-Sionnest and N. F. Scherer. Plasmon-enhanced optical trapping of individual metal nanorods. *Proc. SPIE* **6644** (2007) 66441C.

87. R. Jin, Y. Cao, C. A. Mirkin, K. L. Kelly, G. C. Schatz and J. G. Zheng. Photoinduced conversion of silver nanospheres to nanoprisms. *Science* **294** (2001) 1901.

88. W. Rechberger, A. Hohenau, A. Leitner, J. R. Krenn, B. Lambrecht, and F. R. Aussenegg. Optical properties of two interacting gold nanoparticles. *Opt. Commun.* **220** (2003) 137.

89. P. Jain, W. Huang, and M. A. El - Sayed. On the universal scaling behavior of the distance decay of plasmon coupling in metal nanoparticles pairs: a plasmon ruler equation. *Nano Lett.* **7** (2007) 2080.